The equatorial thermostad and subsurface countercurrents in the light of the dynamics of atmospheric Hadley cells

by Frédéric Marin[1], Bach Lien Hua[1] and Sophie Wacongne[1,2]

ABSTRACT

The simple Held and Hou (1980) nearly inviscid model of the axisymmetric atmospheric circulation, rationalizing the existence of Hadley cells, Jet Streams, and tropical homogenization of potential temperature and vorticity, is adapted to the oceanic subthermocline region. The meridional profile of radiative equilibrium temperature, which provides the driving in the atmospheric case, is replaced, in the oceanic case, by the large-scale equatorial doming of the thermocline. The meridional structure of the equatorial thermostad and the existence, at its poleward flanks, of eastward subsurface countercurrents coincident with sharp potential vorticity gradients are thus explained via angular momentum redistribution by secondary ageostrophic over-turning cells in the meridional plane. Taking into account the existence of the equatorial undercurrent within the thermocline has little effect on the overall structure of the subthermocline solution at a given longitude, even though homogenization of properties is less efficient.

1. Introduction

One of the main features of the zonally-averaged atmospheric circulation is illustrated in Figure 1, which displays the potential temperature and zonal velocity fields in boreal winter from ECMWF data. The large-scale potential temperature field shows a huge equator-pole temperature difference which is the result of the differential radiative balance, mostly visible in the 30–100 kPa pressure range. Equatorward of these strong gradients lies a region of meridionally uniform temperature. Between 0 and 20 kPa, the sign of the meridional temperature gradient weakly reverses and the meridionally uniform temperature region is flanked by two strong eastward jets—the Jet Streams. Held and Hou (1980) (hereafter HH) first proposed an illuminating quantitative model to explain these features: as a consequence of the radiative balance, the equilibrium potential temperature presents a large-scale meridional gradient that creates a geostrophic zonal wind at mid-latitudes; near the equator, angular momentum conservation is violated by this wind field, and ageostrophic meridional cells take place in each hemisphere to redistribute angular momentum in the tropical region. These cells—the Hadley cells—are characterized by rising motion near the equator and strong descent in the subtropics. By using a two-dimensional (2D) model in

1. Laboratoire de Physique des Océans (CNRS-IFREMER-UBO), IFREMER BP 70, 29280 Plouzané, France. *email: lien@ifremer.fr*
2. Department of Oceanography, Florida State University, Tallahasse, Florida, 32306-4320, U.S.A.
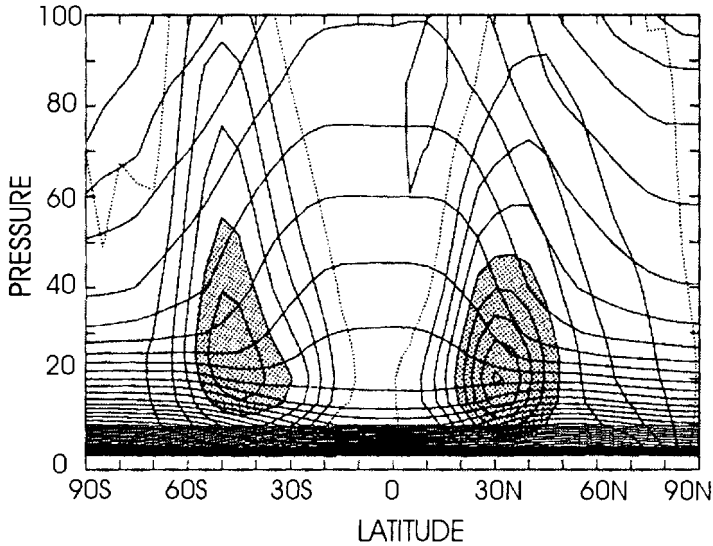
Figure 1. Contours of zonally-averaged zonal wind and potential temperature Θ for December–February based on 6 years of ECMWF data (adapted from James, 1994). Contour interval 5 m s^{-1}, values in excess of 20 m s^{-1} shaded and dotted lines corresponding to westerlies. Contour interval for Θ is 5 K. Note that pressure (in kPa) is running upward to facilitate the comparison with the oceanic case and recall that, unlike temperature, potential temperature increases monotonically as pressure decreases.

the meridional plane, HH were able to relate the extent of the meridional cells to the equator-pole equilibrium temperature difference, and to predict both the meridional homogenization of potential temperature in the tropical region and the amplitude of the Jet Streams that are created at its poleward edges.

Below 200 m in the Pacific Ocean, the distribution of temperature and zonal velocity as seen by SURTROPAC sections at 165E (Fig. 2) shows strong similarities with the atmospheric case: the base of the thermocline appears to shoal from the subtropics to the equator in the southern hemisphere, except in a narrow equatorial region where temperature is homogeneous. This equatorial region is known as the 13°C thermostad, and is flanked at its poleward edges by the eastward flowing SubSurface CounterCurrents (SSCC) near 3° latitude. The large-scale meridional gradients for potential temperature are of opposite sign for the atmosphere and the ocean, the latitudinal scales of the circulation are different (~30° in the atmospheric case, ~3° in the oceanic case) and the presence of the Equatorial UnderCurrent (EUC) within the oceanic equatorial thermocline complicates the picture. Nevertheless, the analogy in the observed distributions suggests an analogy in the dynamics involved. The point of this paper is indeed to explain the characteristics of the equatorial subthermocline by a mechanism analogous to HH based on an equatorial redistribution of angular momentum in response to the large-scale shoaling of the thermocline.
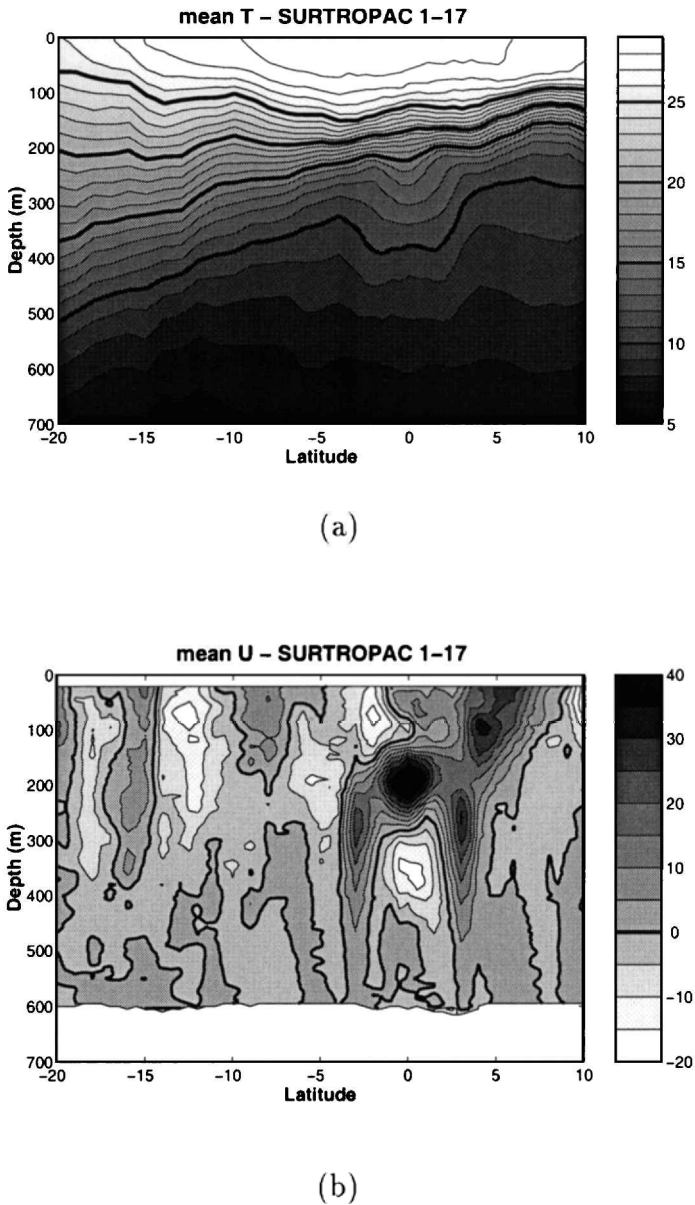
(a)

(b)

Figure 2. Mean values of (a) temperature (°C) and (b) zonal current (cm s^{-1}) from SURTROPAC (1984–1992) at 165E. Information on the data can be found in Delcroix *et al.* (1992).

The bowl-shape of the subtropical thermocline and, in particular, the large-scale upward slope and vertical tightening toward the low latitudes illustrated on Figure 2 has been documented for a long time. The upward sloping is fairly monotonic in the southern hemisphere while interrupted near 10N by a sharp ridge associated with the NECC. This is

discussed for instance by Defant (1936) in his study of the troposphere of the Atlantic Ocean based on the meridional sections of the *Meteor* expedition (1925–1927), and is apparent in the 1972–1973 meridional sections from the GEOSECS program. In the Pacific, the upward sloping, tropical tightening and associated fanning are particularly well represented on the widely cited meridional distribution of mean temperature by Wyrtki and Kilonsky (1984) in the upper 400 m near 155W, based on the 1979–1980 Hawaii-to-Tahiti Shuttle Experiment data. Another salient feature of the tropical thermocline is its zonal slope, upward toward the east. The thermocline, therefore, has a three dimensional structure. Both meridional and zonal slopes are consistent with the large-scale geostrophic wind-driven circulation, the low latitude portions of the subtropical gyres flowing equatorward and westward. The theory of the ventilated thermocline (Luyten *et al.,* 1983), successful at predicting the shape of the thermocline and the strength of the associated geostrophic flow at subtropical latitudes, was first extended to the equatorial zone by Pedlosky (1987) (see also McCreary and Lu (1994) and Liu (1994)). As reviewed by Pedlosky (1996), the solution for the subtropical thermocline depth presents no singularity when the limit of zero latitude is taken. However, the geostrophic balance for the zonal momentum equation fails as the geostrophic meridional velocity becomes infinitely large as latitude tends toward zero. According to Pedlosky (1996), this happens within an equatorial boundary layer, whose width dy is set inertially, and within which the EUC develops. In other words, the theory of the ventilated thermocline, and thus its prediction for the thermocline depth and the fact that both velocity components are in geostrophic balance below the mixed layer, would be valid to within a distance $dy = \sqrt{U/\beta}$ from the equator, i.e., for $U = 1$ m s^{-1} and $\beta = 2. \times 10^{-11}$ m^{-1} s^{-1}, $dy = 2°$ in latitude. However, the theory of the ventilated thermocline does not so far address subthermocline features such as the 13°C thermostad and the SSCCs seen on Figure 2.

The SSCCs, also called Tsuchiya jets, are observed in both Atlantic and Pacific equatorial oceans (Tsuchiya, 1972, 1975; Tsuchiya *et al.,* 1994). They appear as distinct eastward velocity cores (with maxima detached from the EUC maximum) coincident with the meridional density gradients at the poleward edges of the equatorial 13°C thermostad. A complete review can be found in Rowe *et al.* (2000). Johnson and Moore (1997) have documented their zonal evolution in the Pacific Ocean: the SSCCs are found from west to east with relatively constant volume transports, even though they appear to shoal and depart from the equator when they cross the equatorial basin. Gouriou and Toole (1993) described them as the location of strong meridional gradients of properties such as potential vorticity and tracers, suggesting that the SSCCs act as a barrier to the meridional flow. This view is reinforced by Rowe *et al.*'s (2000) recent data analysis, which reveals much sharper zonal velocity profiles and potential vorticity fronts through the use of stream coordinates. Tsuchiya (1981) used maps of properties on isanosteric surfaces to suggest that the characteristics of the 13°C water are acquired in the northeast of New Zealand and in the Tasman Sea by convection and are then advected equatorward. A similar process is found by Tsuchiya (1986) in the Atlantic Ocean.

McPhaden (1984) first proposed a theory for the dynamics of the SSCCs. With a linear and vertically diffusive model, he explained these jets as diffusive extensions of the EUC, at the poleward edge of a diffusive equatorial vorticity boundary layer broader than the diffusive momentum one. The induced planetary vorticity advection is balanced by vortex stretching that weakens the temperature stratification: a thermostad is then formed and the SSCCs appear as the geostrophic response to this thermostad. However, a diffusive theory cannot explain a local maximum in zonal velocity at the core of the SSCCs; nonlinearities must play a part. Comparing idealized linear and nonlinear responses of the equatorial ocean to zonal winds as obtained numerically by Philander and Pacanowski (1980), McPhaden noticed indeed that the SSCCs become distinct from the EUC in the nonlinear run. He invoked the need for poleward flow at the base of the EUC. Assuming an *a priori* eastward jet in the western part of the basin, Johnson and Moore (1997) explained the SSCCs zonal evolution by using an inertial jet model based on conservation of both Bernoulli function and potential vorticity. They successfully related the poleward shift of the jets to the eastward shoaling of the tropical thermocline, however without addressing the mechanism that initially creates the SSCCs.

In this paper, we address the formation mechanism of the SSCCs and the thermostad, neglecting the dynamics of the zonal evolution, in contrast with Johnson and Moore (1997), and we focus on nearly inviscid dynamics in contrast with McPhaden (1984). We will be arguing, by analogy with the atmospheric case, that geostrophic balance for the zonal momentum equation fails over an equatorial latitude range wider than Pedlosky's inertial boundary layer, within which an angular momentum conserving secondary flow takes place. We will start from a profile of thermocline depth consistent with the ventilated thermocline theory all the way to the equator (the analog of the profile of radiative equilibrium temperature in the atmosphere), and let a secondary circulation develop to redistribute angular momentum (the analog of the Hadley cell). The width of the zone so homogenized will be of the order of an equatorial radius of deformation; i.e., 3 degrees latitude (the analog of the 30 degrees latitude of the atmospheric case) and it will be bounded by eastward jets, the subsurface countercurrents (the analogs of the Jet Streams). We will restrict our attention to a problem strictly symmetric with respect to the equator.

Section 2 extends the main results that were obtained by HH to the oceanic case. With the same minimal assumptions as HH, the equatorial recirculation implied by angular momentum redistribution is assumed to take place in the meridional plane, and a 2D model presented in Section 3 is used. Section 4 presents numerical results for the oceanic subthermocline when the contribution of the zonal gradients is neglected, in strict analogy to the HH model (cases with zero or westward surface flows are considered). In Section 5, zonal gradients are parameterized in the zonal momentum equation as a forcing term that creates the EUC at thermocline levels, and the interactions between the oceanic equivalents of the Hadley cells and the EUC are discussed. Section 6 summarizes and discusses the results of this paper.

2. Held and Hou theory for the oceanic case

Using a 2D model in the meridional plane, HH describe the Jet Streams and the meridional homogenization of potential temperature in the tropical atmosphere as the response, via an angular-momentum conserving circulation, to the large-scale meridional gradient in potential temperature imposed by radiative equilibrium.

In this section, a similar approach is used for the oceanic case. In the ocean, a large-scale meridional gradient in density is also observed, due to the large-scale shoaling of the pycnocline from the subtropics to the equator caused by ventilation. The large-scale density field $\bar{\rho}$ is seen to vary quasi-linearly in $y - z$ in the tropical region (see Fig. 2(a) or Tsuchiya, 1994), in agreement with the thermocline depth deduced by Luyten *et al.* (1983) from their 2½-layer ventilated model (to the west of an eventual shadow zone in layer 2)

$$h^2(x, y) = \frac{(D_0^2(x, y) + H_2^2)}{\left(1 + \frac{\gamma_1}{\gamma_2}(1 - |y|/y_2)^2\right)}.$$ (1)

Here y_2 is the latitude of subduction for layer 2, γ_1 and γ_2 are the reduced gravities for layer 1 and 2, respectively; H_2 is the thickness of layer 2 at the eastern boundary at $y = y_2$ and $D_0^2(x, y)$ is proportional to the Ekman pumping integrated from the eastern boundary. Under the assumption that the windstress is essentially zonal and independent of the latitude in the tropical region, D_0^2 is no longer a function of y and the thermocline depth then behaves as

$$\left(\frac{\gamma_2}{\gamma_1 + \gamma_2}\right)^{1/2} \times (D_0^2(x) + H_2^2)^{1/2} \times \left(1 + \frac{\gamma_1}{\gamma_1 + \gamma_2}\frac{|y|}{y_2}\right)$$

when $|y| \to 0$, i.e. linearly in $|y|$. In particular, as remarked by Pedlosky (1996), the thermocline depth deduced from the ventilation theory is well behaved when one approaches the equator.

For the sake of simplicity, $\bar{\rho}$ is assumed to be symmetric with respect to the equator and is chosen of the form

$$\bar{\rho}(y, z) = F(z + \alpha|y|),$$ (2)

over a domain extending from the base of the mixed layer (considered as $z = 0$) to the base of the thermocline ($z = -H_{TH}$). The coefficient α is constant and represents the meridional slope of the thermocline. F is an *a priori* arbitrary function, which we choose to be linear. At the equator ($y = 0$), F is related to the mean thermocline Brunt-Väisälä frequency $\mathcal{N}^2$ by $F(z) = -(\rho_0/g)\mathcal{N}^2 z$, where $\mathcal{N}^2$ is taken as a constant and where ρ_0 is the mean reference value for the density; therefore the form of F is given by $F(z + \alpha|y|) = -(\rho_0\mathcal{N}^2/g)(z + \alpha|y|)$. Such a formulation yields the required large-scale shoaling of the thermocline, which is seen in Figure 2(a) and which constitutes our ventilation constraint (in analogy with the radiative heating constraint of the atmospheric case).

The geostrophic velocity $\tilde{u}$ implied by (2) can be deduced from the thermal wind balance:

$$\frac{\partial \tilde{u}}{\partial z} = \frac{g}{\beta y \rho_0} \frac{\partial \tilde{\rho}}{\partial y} = -\frac{\alpha}{\beta |y|} \mathcal{N}^2, \tag{3}$$

yielding

$$\tilde{u}(y, z) - \tilde{u}(y, -H_{\mathrm{TH}}) = -\frac{\alpha}{\beta |y|} \mathcal{N}^2 (z + H_{\mathrm{TH}}). \tag{4}$$

The geostrophic velocity is singular at the equator so that different dynamics must take place in an equatorial region.

In the atmospheric case, the situation is different. In contrast with the linear dependence of the thermocline depth with latitude due to the dynamics of the ventilation in the oceanic case, the large-scale potential temperature Θ_E in the atmosphere presents a parabolic dependence in y ($\Theta_E = \Theta_{E0} - (\Delta\Theta/a^2)y^2$ at a given depth, a being the Earth's radius and $\Delta\Theta$ the pole-equator temperature difference) as the result of radiative equilibrium. The vertical gradient for the geostrophic velocity u_E is then constant and $u_E = (2g\Delta\Theta/\beta a^2 \Theta_0)z$ presents no singularity at the equator. Therefore, ($u = u_E$, $\Theta = \Theta_E$) is a stationary solution of the motion equations for the atmosphere in the absence of dissipation. However, in presence of viscosity (no matter how small), it cannot be a steady solution for the symmetric equations of motion. Indeed, according to Hide (1969), the absolute angular momentum $\tilde{M} = (\beta/2)a^3 + a(u - (\beta/2)y^2)$ (under the β-plane assumption) cannot have a maximum in the fluid interior in presence of viscous terms. Its extremum value must occur at the ground, where it coincides with the angular momentum of the solid earth[3]

$$\frac{\beta a}{2}(a^2 - y^2) \leq \frac{\beta a^3}{2}. \tag{5}$$

Now $u_E = (2g\Delta\Theta/\beta a^2 \Theta_0)z$ implies westerlies at the equator, i.e. positive M that, at $y = 0$, increases with height, which is forbidden by Hide's argument.

So, in the ocean as in the atmosphere, the zonal thermal wind solution implied either by the ventilation constraint or by the radiative equilibrium constraint, cannot be a solution in the vicinity of the equator. An initial condition based on such constraints is unstable, causing a secondary circulation to develop. In the atmosphere, a convective meridional cell indeed takes place to redistribute angular momentum near the equator so that Hide's argument is satisfied. In the ocean, we can assume that a redistribution mechanism similarly based on angular momentum conservation occurs in the meridional plane, and explore the consequences of our assumption. At the base of the thermocline, far from the viscous mixed layer, the zonal velocity u_M deduced from angular momentum conservation

---

3. In the remainder of the paper, we redefine angular momentum as $M = (1/a)[\tilde{M} - (\beta/2)a^3] = u - (\beta/2)y^2 \leq 0$.

would be:

$$u_M(y, z = -H_{\text{TH}}) = \frac{\beta}{2} y^2 + u_{EQ}, \tag{6}$$

where u_{EQ} is the zonal velocity at the equator at the base of the mixed layer. Thus u_M exhibits a characteristic meridional profile which is quadratic, and, averaged over the vertical, the corresponding density field $\overline{\rho}_M$ follows from thermal wind balance

$$\frac{g}{\rho_0} \frac{\partial \overline{\rho}_M}{\partial y} = \beta y \frac{\partial u_M}{\partial z} \sim \beta y \frac{u(z = 0) - u_M(z = -H_{\text{TH}})}{H_{\text{TH}}} = -\frac{\beta^2 y^3}{2 H_{\text{TH}}}, \tag{7}$$

assuming negligible variation in latitude of the surface current over the region of interest.
   Hence,

$$\overline{\rho}_M(y) = \overline{\rho}_{M_0} - \frac{\beta^2 \rho_0}{8 g H_{\text{TH}}} y^4, \tag{8}$$

where $\overline{\rho}_{M_0} = \overline{\rho}_M(y = 0)$.
   The density that is implied by conservation of angular momentum follows a y^4 law, a much flatter profile, near $y = 0$, than the linear profile for the ventilated thermocline: one effect of the angular momentum redistribution is to meridionally homogenize the potential temperature field in the vicinity of the equator.
   Following HH,[4] the meridional extent Y of the equatorial Hadley cell can then be obtained from two arguments. The first one is an argument of continuity of the heat content, $\int_{-H_{\text{TH}}}^0 \rho(Y, z)\, dz = \int_{-H_{\text{TH}}}^0 \overline{\rho}_M(Y)\, dz$, i.e.

$$\frac{\rho_0 \mathcal{N}^2}{g} \left| \frac{H_{\text{TH}}^2}{2} - \alpha Y H_{\text{TH}} \right| = \overline{\rho}_{M_0} H_{\text{TH}} - \frac{\rho_0 \beta^2}{8g} Y^4. \tag{9}$$

If we assume, furthermore, that heat exchange between the local Hadley cells and the subtropics can be neglected as a first step, the second one is an argument of no net heating over the domain, $\int_Y^0 \int_{-H_{\text{TH}}}^0 \rho(y, z)\, dy\, dz = \int_Y^0 \int_{-H_{\text{TH}}}^0 \overline{\rho}_M(y)\, dy\, dz$, i.e.

$$\frac{\rho_0 \mathcal{N}^2}{g} \frac{H_{\text{TH}}^2}{2} Y - \alpha \frac{\rho_0 \mathcal{N}^2}{2g} H_{\text{TH}} Y^2 = \overline{\rho}_{M_0} Y H_{\text{TH}} - \frac{\rho_0 \beta^2}{40g} Y^5. \tag{10}$$

   Y is thus given by

$$Y^3 = \frac{5 \alpha \mathcal{N}^2 H_{\text{TH}}}{\beta^2}, \tag{11}$$

___

4. HH theory is derived more simply for Cartesian coordinates in James (1994, pp. 80–111).

or, if we note $\Delta\rho$ the density jump across the thermocline,

$$Y^3 = \frac{5g\alpha\Delta\rho}{\rho_0\beta^2}. \tag{12}$$

A typical value for the density jump across the thermocline is $\Delta\rho \sim 2$, and the large-scale slope of the thermocline is of order 150 m for 10° latitude, so that $\alpha \sim 1.5 \times 10^{-4}$. An estimate of the meridional extent of the oceanic Hadley cells is then $Y = 2.9°$, which is consistent with the meridional extent of the oceanic thermostad. The value of Y is found to be close to the first equatorial radius of deformation and is wider than the 2° half-width of a 1 m s^{-1} inertial undercurrent.

An estimate of the eastward jets at the poleward edges of the meridional overturning cell is then:

$$u_M(Y, -H_{\text{TH}}) - u_{EQ} = \frac{\beta}{2}Y^2, \tag{13}$$

i.e. $u_M(Y, -H_{\text{TH}}) \sim 100$ cm s^{-1} for $u_{EQ}(z = 0) = 0$, given the values of $\Delta\rho$ and α mentioned above. If the equatorial velocity at the base of the mixed layer is westward instead, the estimate of $u_M(Y, -H_{\text{TH}})$ is less. For instance, $u_{EQ} = -25$ cm s^{-1} implies $u_M(Y, -H_{\text{TH}}) \sim 75$ cm s^{-1}.

Thus, the application of the HH theory to the oceanic case gives a rationale for the meridional extent of the oceanic Hadley cells analogs and the latitude of the oceanic Jet Streams analogs at their poleward edges. Both Y and u_{SSCC} are determined exclusively by the large-scale meridional slope induced by the ventilation and the density jump across the thermocline. The meridional width Y associated with the angular momentum redistribution is seen to be close to the equatorial radius of deformation, unlike the meridional width of the EUC which is inertial. The scaling with the radius of deformation has already been noticed by Condie and Rhines (1994), for topographic Hadley cells, in laboratory experiments where the bottom topography provided a convenient way for establishing radial temperature gradients. In their case as in ours, the Hadley cell width is limited by the tendency to conserve angular momentum.

The same arguments applied to the atmospheric case lead to the following estimates for the meridional extent Y_{ATM} of the Hadley cell and the amplitude u_{JET} of the Jet Streams:

$$Y_{\text{ATM}} = \left|\frac{20gH\Delta\Theta}{3\beta^2a^2\Theta_0}\right|^{1/2}, \tag{14}$$

$$u_{\text{JET}} = \frac{\beta}{2}Y_{\text{ATM}}^2 = \frac{10gH\Delta\Theta}{3\beta a^2\Theta_0}, \tag{15}$$

both estimates depending only on the equilibrium equator-pole temperature difference[5] $\Delta\Theta$ and on the height H of the atmosphere conserved by angular momentum redistribution.

With $\Theta_0 = 255K$, $\Delta\Theta = 40K$ and $H = 15 \times 10^3$ m (Lindzen, 1990), the theoretical meridional extent of the atmospheric Hadley cells is 2800 km and the amplitude of the Jet Stream is about $u_{JET} \sim 85$ m s^{-1}.

Thus, the HH symmetric solution predicts a finite meridional extent for the Hadley cells and yields a jet at about the right place in both ocean and atmosphere. In the ocean, the estimate of the meridional extent of the Hadley cells analogs yields encouraging results when compared to the observations, but the amplitude of the oceanic Jet Streams proves to have too large an amplitude. In the atmosphere, the intensity of the Hadley cells proves to be weaker than what is observed and the magnitude of the Jet Streams is far too large (Lindzen, 1990), suggesting that the asymmetry about the equator between the winter and summer hemispheres (Lindzen and Hou, 1988) and the eddies that are neglected in a 2D model play a quantitative role for the fully three-dimensional solution.

3. Formulation of the problem

The two main ingredients of HH theory yielding our analytic predictions for Y and $u_M(Y)$ have been the angular momentum conserving character of the secondary circulation and the assumption that the Hadley cells are thermally insulated from the subtropics. Only a fully three-dimensional framework, delayed to a subsequent publication, will allow a definitive test of these assumptions in the oceanic case. In this section, we formalize how to parameterize within a 2D framework the effects of the 3D oceanic circulation, and clarify where the above assumptions enter the problem.

The large-scale flow associated with the prescribed density field $\bar{\rho}(x, y, z)$, denoted by $\sim$, is assumed to be stationary, in geostrophic balance, hydrostatic and incompressible

$$\beta y \tilde{u} = -\frac{1}{\rho_0} \tilde{p}_y, \tag{16a}$$

$$\tilde{p}_z + \tilde{\rho} g = 0, \tag{16b}$$

$$\tilde{u}\bar{\rho}_x + \tilde{v}\bar{\rho}_y + \tilde{w}\bar{\rho}_z = \mathscr{D}_v(\bar{\rho}), \tag{16c}$$

$$\tilde{u}_x + \tilde{v}_y + \tilde{w}_z = 0. \tag{16d}$$

The equatorial β-plane approximation is made, and $\mathscr{D}_v$ refers to the dissipation operator (assumed to be linear).

Once $\bar{\rho}$ is set, the three components $(\tilde{u}, \tilde{v}, \tilde{w})$ of the velocity and the pressure $\tilde{p}$ are completely determined by (16). The equation for the zonal momentum enters the problem only implicitly through the choice of $\bar{\rho}$. In the subtropics, the large-scale observed density

---

5. Both $\Delta\Theta$ in the atmosphere and $\alpha\Delta\rho$ in the ocean correspond to a lateral, rather than vertical, temperature difference of the large-scale flow.

field is close to the value prescribed by ventilation theory, and both zonal and meridional momentum equations are in geostrophic balance. However, as one approaches the equator, there is a latitude where a geostrophic balance for the zonal momentum equation no longer holds: a secondary flow has to take place in the final flow. We shall denote the secondary flow by (u', v', w', p', ρ') and the total flow by (u, v, w, p, ρ), e.g. $u = \tilde{u} + u'$, etc. The total flow is a solution of the complete primitive equations

$$u_t + uu_x + vu_y + wu_z - \beta yv = -\frac{1}{\rho_0} p_x + \mathscr{D}_v(u), \tag{17a}$$

$$v_t + uv_x + vv_y + wv_z + \beta yu = -\frac{1}{\rho_0} p_y + \mathscr{D}_v(v), \tag{17b}$$

$$p_z + \rho g = 0, \tag{17c}$$

$$\rho_t + u\rho_x + v\rho_y + w\rho_z = \mathscr{D}_v(\rho), \tag{17d}$$

$$u_x + v_y + w_z = 0. \tag{17e}$$

Eqs. (17b) and (17c) can be replaced by an equation for the zonal component of vorticity $\zeta = -v_z$

$$\zeta_t + u\zeta_x + v\zeta_y + w\zeta_z + \frac{g}{\rho_0} \rho_y - \beta yu_z + u_xv_z - u_zv_x = -[\mathscr{D}_v(v)]_z. \tag{18}$$

In this paper, the 2D framework of HH is kept by assuming that the zonal variations of only the secondary flow can be neglected

$$u'_x = v'_x = w'_x = \rho'_x = p'_x = 0, \tag{19}$$

while the 3D character of the large-scale flow is retained (in particular $\tilde{p}_x$ is not required to be zero at any depth). Under this assumption, the incompressibility condition reduces to

$$v'_y + w'_z = 0, \tag{20}$$

and a streamfunction ψ' for displacement in the meridional plane can be defined, such that

$$v' = -\psi'_z, \qquad w' = \psi'_y, \qquad \zeta' = \psi'_{zz}. \tag{21}$$

The advection operator associated with the secondary flow is thus $d/dt = \partial/\partial t + J(\psi', .)$ where J is the Jacobian $J(a, b) = a_y b_z - a_z b_y$.

Subtracting (16c) to (17d), we obtain the equation for the total density

$$\rho_t + J(\psi', \rho) = -\tilde{v}\rho'_y - \tilde{w}\rho'_z - u'\tilde{\rho}_x + \mathscr{D}_v(\rho'), \tag{22}$$

which is forced by (i) the advection of the secondary density field by the large-scale meridional flow, which could cause a net heat exchange with the subtropics, and (ii) the advection of the large-scale density field by the zonal secondary velocity. In this study it is

assumed that these forcings mainly act to maintain the total density close to the large-scale density field, and that they can be parameterized by a relaxation term of the form $-r_\rho \rho'$, so that an exact steady solution, in presence of the relaxation term, is $\rho = \bar{\rho}$, when neglecting both viscous effects and secondary circulation ($v' = w' = 0$). Such a choice, which replaces nonlinear transport terms in (22) by a linear expression, implies that there is no net heat exchange between the equatorial region and the subtropics, a restriction inherent to our 2D framework. A Rayleigh relaxation is used throughout Sections 5 and 6a, but other forms are tested in Section 6b. Because we consider that the large-scale meridional velocity and the zonal density gradient are due to thermocline ventilation, they vanish beneath the thermocline. The relaxation term is thus chosen to be zero in the subthermocline. The subthermocline region of interest is therefore driven from above, in contrast to the atmospheric case where the forcing acts throughout the entire height of the domain.

The zonal momentum equation for the total flow

$$u_t + J(\psi', u) - \beta y v' = -\frac{1}{\rho_0}\tilde{p}_x + \beta y \tilde{v} - u\tilde{u}_x - \tilde{v}u_y - \tilde{w}u_z + \mathscr{D}_\nu(u) \quad (23)$$

is forced by both the geostrophic imbalance between the meridional velocity and the zonal pressure gradient, and the interactions between the total zonal velocity and the large-scale circulation. The geostrophic imbalance is supposed to be negligible everywhere except in the immediate vicinity (both in y and z) of the EUC, where it is exactly balanced by the advection of zonal velocity by the large-scale flow and by the dissipation of the large-scale flow

$$u_{\mathrm{EUC}}(u_{\mathrm{EUC}})_x + \tilde{v}(u_{\mathrm{EUC}})_y + \tilde{w}(u_{\mathrm{EUC}})_z - \beta y \tilde{v} = -\frac{1}{\rho_0}\tilde{p}_x + \mathscr{D}_\nu(u_{\mathrm{EUC}}) \qquad (24)$$

(Pedlosky, 1988).

As in Eq. (22), the forcing terms in (23) are parameterized by a relaxation term $-r_u(u - u_{\mathrm{EUC}})$ which only acts in the thermocline and within a narrow equatorial band, where u_{EUC} is chosen to correspond to the observations. In the same way as for the density, the choice of a linear relaxation term implies no net angular momentum exchange between the equatorial region and the subtropics. Because ($u = \tilde{u}$, $\psi' = 0$) is expected to be a solution of the zonal momentum equation in the subtropics, the relaxation term must be vanishingly small far from the equator. Similarly, the action of the large-scale flow in the zonal vorticity equation (18) is parameterized by a relaxation term ($-r_\psi \psi'_{zz}$) toward a state of no secondary circulation, whose effect turns out to be negligible.

The problem that has to be solved within a 2D framework in y and z becomes

$$u_t + J(\psi', u) - \beta y v' = \mathscr{D}_\nu(u - u_{\mathrm{EUC}}) - r_u(u - u_{\mathrm{EUC}}), \qquad (25a)$$

$$(\psi'_{zz})_t + J(\psi', \psi'_{zz}) - \beta y u'_z + \frac{g}{\rho_0}\rho'_y = [\mathscr{D}_\nu(\psi'_z)]_z - r_\psi \psi'_{zz}, \qquad (25b)$$

$$\rho_t + J(\psi', \rho) = \mathscr{D}_\nu(\rho') - r_\rho \rho'. \qquad (25c)$$

It is now apparent that, if or where the relaxation term $-r_u(u - u_{EUC})$ is zero, Eq. (25a) does conserve angular momentum (apart from dissipative terms), given our assumption that $p'_x = 0$.

The system (25) is solved in a $[-LL] \times [-H0]$ rectangular domain, with the following boundary conditions at the bottom $(z = -H)$, the surface $(z = 0)$, and the southern $(y = -L)$ and northern $(y = L)$ boundaries:

$$\text{at } y = \pm L \quad u = \tilde{u} \quad \rho_y = \tilde{\rho}_y, \quad \psi' = 0, \quad w' = \psi'_y = 0, \qquad (26a)$$

$$\text{at } z = -H \quad u = 0, \quad \rho = \tilde{\rho}, \quad \psi' = 0, \quad v'_z = \psi'_{zz} = 0, \qquad (26b)$$

$$\text{at } z = 0 \quad u = u_{SURF}, \quad \rho_z = 0, \quad \psi' = 0, \quad v'_z = -\psi'_{22} = 0. \qquad (26c)$$

At the poleward boundaries, the zonal velocity is assumed to remain in geostrophic balance, and the vertical velocity for the secondary flow is set to zero. At the bottom, the boundary condition is one of no flux for the meridional secondary velocity, and zonal velocity and density are chosen to remain equal to those prescribed by the large-scale field. At the surface, because we have no means to set the wind stress as a boundary condition in a 2D model, we prescribe u arbitrarily, and conditions of no flux for density and meridional secondary velocity are assumed. Finally $\psi' = 0$ at all boundaries because the secondary circulation is anticipated to be mostly confined to the equatorial thermocline. It must be noted that the choice of $v' = 0$ instead of $v'_z = 0$ at the surface and bottom has also been tried and produces no significant change. Although x does not appear explicitly, the solution will depend on x through the specification of u_{EUC} and $\tilde{\rho}$.

Steady-solutions of (25–26) are sought in a given meridional plane at $x = x_0$, for $H = 700$ m and $L = 1000$ km; they should be representative of the time-mean circulation near the equator, at that longitude. One possible solution is the thermal-wind velocity implied by the large-scale latitudinal shoaling of the thermocline, with $(v' = w' = 0)$. Another solution is such that a secondary meridional circulation takes place $(v', w' \neq 0)$ to accommodate boundary conditions. In that case one obtains a different zonal velocity field. The problem is run as an initial-value problem starting from rest with $\rho = \tilde{\rho}(x_0, y, z)$ to determine which solution actually takes place.

We now choose a $\tilde{\rho}(x_0, y, z)$ field that resembles the observations, i.e. a thermocline that shoals linearly toward the equator while becoming thinner, a feature consistent with PV conservation. We thus prescribe at 9S and 9N a tanh vertical profile centered at 350 m and yielding a 150 m-thick thermocline, and at the equator another tanh vertical profile centered at 200 m and yielding a 50 m-thick thermocline. These profiles are then linearly connected. The density jump across the thermocline is chosen to be $\Delta\rho = 2.6$, and the Brunt-Väisälä frequency of the deep ocean is taken as 3.10^{-3} s^{-1}. The above values are inspired by the Pacific observations. The resulting field is presented on Figure 3(a) for a case without EUC.
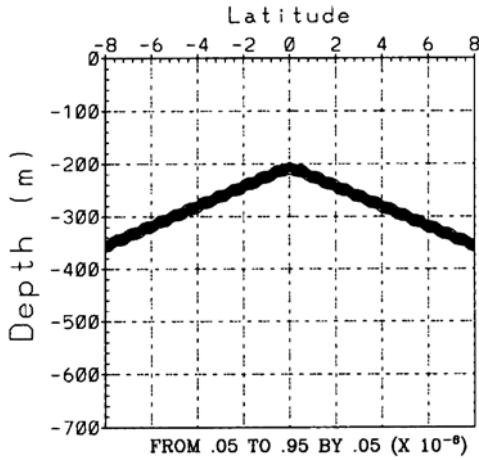
The relaxation coefficient r_ρ of the density field toward the large-scale ventilated density field is presented in Figure 3(b). It is maximum above the thermocline where its value is set at $r_\rho = 10^{-6}$ s^{-1}, which corresponds to a minimum relaxation time of $\tau_\rho \sim 12$ days, and

LARGE–SCALE DENSITY

(a)
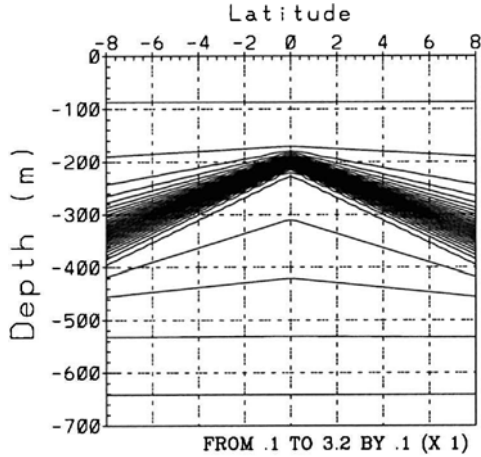
RAYLEIGH

(b)

Figure 3. (a) Large-scale density field $\tilde{\rho} - \rho_0 + \Delta\rho$. (b) Rayleigh coefficient r_ρ for the density field. Unit is 10^{-6} s^{-1}. Maximal value of r_ρ is reached at the surface.

vanishes beneath the thermocline where the ventilation does not act. The choice of 12 days will be justified *a posteriori* in Subsection 4(a). The relaxation coefficient r_u must be vanishingly small in the subtropics, so that it acts exclusively in a narrow equatorial region, where we set it equal to r_p.

Finally the dynamics of the subthermocline is supposed to be only weakly dissipative, which is made possible by the fine vertical resolution of the model grid (typically 10 m). $\mathscr{D}_v$ is chosen of a Laplacian form: the lateral viscosity coefficient is set constant at $\nu_y = 10$ m^2 s^{-1} throughout the paper, while the vertical viscosity coefficient has an exponential profile, in order to simulate a surface-intensified frictional layer:

$$\nu_z = \nu_b + \nu_s \exp{(z/z_v)} \tag{27}$$

with $\nu_b = 3.10^{-5}$ m^2 s^{-1}, $\nu_s = 5.10^{-4}$ m^2 s^{-1} and $z_v = 40$ m.

Let us emphasize the two main differences between the atmospheric and oceanic cases. First the ventilation only acts within the thermocline portion of the domain of interest, while the forcing in density due to radiative balance is throughout the atmosphere. Second, the angular momentum M is not conserved everywhere because of the x-dependent forcing term within the equatorial oceanic thermocline in a narrow equatorial band, whereas M is strictly conserved, apart from dissipative terms, in the atmospheric case studied by HH.

We shall address these two differences by first considering the strictly angular momentum preserving dynamics (Section 4) and then by taking into account the existence of the EUC (Section 5).

4. Angular momentum preserving dynamics

In this section, the closest analog of the atmospheric case is studied by setting $r_u = 0$ and $u_{\text{EUC}} = 0$ in (25a). It is well documented in HH theory that the final wind distribution strongly depends upon the interactions between the Hadley cells and the ground viscous boundary layer. In our case, the sea surface mixed layer plays an analogous role.

a. Case of zero surface flow

The simplest assumption for the boundary condition at the surface which ensures a viscous boundary layer is to set $u_{\text{SURF}} = 0$.

Figure 4 illustrates the steady-state solution found in that case. Note the strong resemblance between Figure 4(a)–(b) and Figure 1. Eastward jets are formed near 3° latitude in each hemisphere at the base of the thermocline. These jets reach an amplitude close to 87 cm s^{-1} in the steady-state solution, but they appear very quickly in the numerical simulations (in less than 30 days), when compared to the equilibration time of about 2000 days, which results from the low vertical viscosity used in the model. Easterly winds (dotted lines in Fig. 1) and westward currents (dashed lines in Fig. 4(a)) occur near $y = 0$ in both the atmosphere and the ocean, in agreement with Hide's argument. Between 3S and 3N the density is meridionally homogenized to form a thermostad, just like the
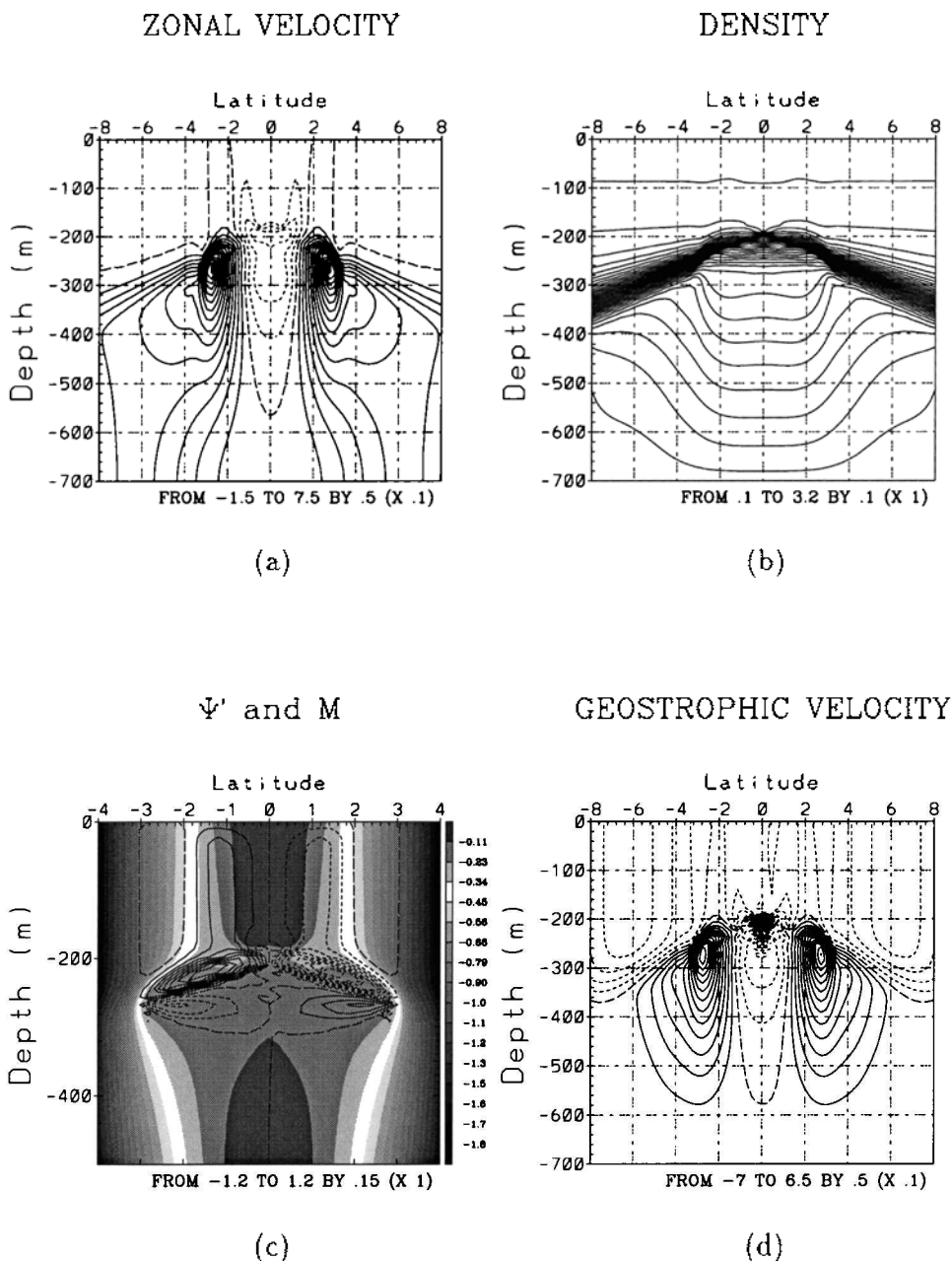
ZONAL VELOCITY

DENSITY

Ψ' and M

GEOSTROPHIC VELOCITY

Figure 4. Results for $u_{SURF} = 0$ and without EUC. Fields of total zonal velocity u in m s^{-1} (a), total density $\rho - \rho_0 + \Delta\rho$ (b), angular momentum (grey) and secondary overturning streamfunction ψ' (solid: >0 and dashed: <0) (c), and geostrophic velocity (d) for a reference level at $z = -H$. The zero isoline is long-dashed.

potential temperature field displays little latitudinal variations in the tropical atmosphere. In the lower thermocline, this homogenization is the product of the overturning cells developed by the secondary circulation, the oceanic Hadley cells analogs, which are strongest within the thermocline in the depth range [200–270 m] (Fig. 4(c)). Below the thermocline, the density is unforced; therefore, in contrast with the atmospheric case, free transient gravity oscillations, visible in ψ' at early stages, are excited in the numerical solutions. This results in a geostrophic adjustment of the deeper layers, with, in the final state, an homogenized layer between 250 m and 400 m bounded by strong meridional density gradients in thermal wind balance at its poleward flanks (compare Fig. 4(d) to 4(a)).

Figure 4(c) displays a zoom between 4S and 4N and $z \leq 500$ m of both the secondary circulation ψ' and contours of the angular momentum M. The sense of rotation of the overturning cells implies net descent of fluid parcels in the thermocline at the equator. Along the upper and lower branches of the thermocline overturning cells, isolines of the two fields are fairly parallel, thus illustrating the angular momentum conserving character of the dynamics involved. This is corroborated by Figure 5(a) that compares the zonal velocity at the depth of the SSCCs maxima ($z = -270$ m) to the zonal velocity deduced from angular momentum conservation $u_M = (\beta/2)y^2$ (Eq. 6, with $u_{EQ} = 0$). These two curves display a very close correspondence up to $|y| = 3.2°$, with a vertical shift that reflects the existence of a westward flow at the base of the mixed layer, and a sharp transition to much weaker subtropical velocities beyond $|y| = 4°$.

The steady nearly inviscid recirculation cells displayed on Fig. 4(c) constitute another example of the type of 2D closed-streamline flows studied by Batchelor (1956). These flows are known to homogenize any conservative scalar field that they enclose by expelling gradients to their periphery, insofar as the majority of the streamlines do not pass through the viscous boundary layer at the surface, thereby allowing the application of the Prandt-Batchelor theorem (see also Cessi, 1998). Figure 4(c) illustrates indeed the weakening of M gradients equatorward of 3° and their concentration at 3S and 3N.

The interaction between the cells and the density field (which is not strictly conserved because of the relaxation term within the thermocline, see Eq. (25c)) is illustrated on Figure 5(b), which displays the depths of a given isopycnal surface for both $\tilde{\rho}$ and ρ. The functions displayed on Figure 5(b) also represent, within a positive multiplicative factor, the meridional profiles of the large-scale and final thermoclines. Figure 5(b) illustrates that, for $|y| < 2°$, relaxation toward the ventilated density field cools the fluid ($-r_\rho \rho' > 0$), which is consistent with the sense of rotation of the overturning cells. This slanted convective circulation does not imply static instability ($\mathcal{N}'^2 = -(g/\rho_0)(\partial \rho/\partial z)$ remains positive). Note the y^4 dependence in the case of ρ, in contrast with the linear y-dependence in the case of $\tilde{\rho}$.

The argument of no net heating is not valid for a given isopynal (e.g. the areas between the two curves of Figure 5(b) are not equal); yet this argument still holds when considering

Journal of Marine Research

U (z = -270m)

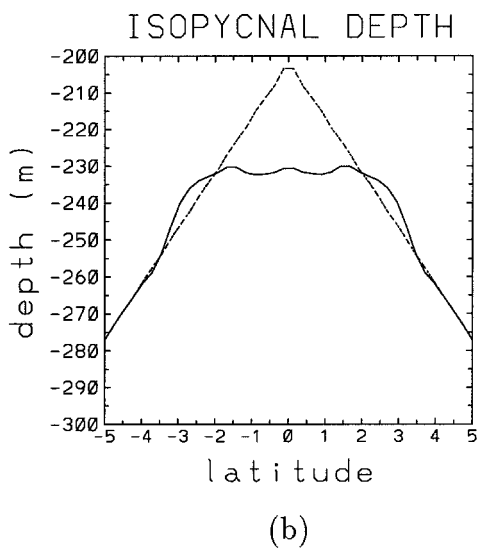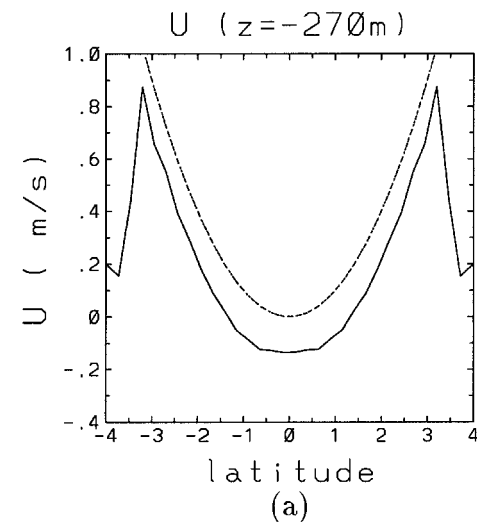

(a)

ISOPYCNAL DEPTH

(b)

Figure 5. (a) Latitudinal section of total zonal velocity u at $z = -270$ m (solid) and velocity deduced from angular momentum conservation (dashed); (b) initial (dashed) and final (solid) depth of the isopycnal $\rho = \rho_0 + 1.7$ for the same simulation as Figure 4.

the depth-averaged density distribution within the forced region (i.e. we have numerically checked that $\int\int r_\rho \rho \, dz \, dy = \int\int r_\rho \rho \, dz dy$ for $r_\rho > 0$).

Recall that, by definition, the secondary velocities (v', w') associated with the overturning cells are distinct from the total fluid parcels velocities. Orders of magnitude are $v' \sim$ 4 cm s^{-1} and $w' \sim 6 \times 10^{-6}$ m s^{-1}, which, given the dimensions of the cells, leads to an overturning time scale of about 400 days.

We now turn to the interaction between the cells and the field of Ertel Potential Vorticity $\mathcal{Q}_E = (g/\rho_0)J(M, \rho) = -(g/\rho_0)\rho_z(f - u_y) - (g/\rho_0)u_z\rho_y$ (Fig. 6). Note that, because of ρ, $\mathcal{Q}_E$ is not strictly conserved either. Large-scale (computed with the large-scale thermal wind velocity, set to zero at the bottom) and final fields of $\mathcal{Q}_E$ are displayed on Figure 6(a) and 6(b), and meridional sections at $z = -270$ m are shown on Figure 6(c) and 6(d). Figure 6(a) shows a large region, in the upper thermocline and equatorward of about 2 degrees in latitude, where $f\mathcal{Q}_E < 0$, suggesting that inertial instability[6] plays a quantitative role to trigger the secondary circulation (Hua *et al.,* 1997). This is corroborated by the rapid appearance of eastward jets in the numerical simulations: the formation time of 30 days is indeed much shorter than both the homogenization time scale of 400 days and the diffusive time scale of 2000 days. The overturning cells recognize $\mathcal{Q}_E$, by expelling its gradients near 3° and by setting $\mathcal{Q}_E$ to zero in the upper part of the thermostad (Fig. 6(b)). This zero value follows from $\mathcal{Q}_E$ definition: $\mathcal{Q}_E = (g/\rho_0)\mathbf{i} \cdot \nabla M \times \nabla\rho$ ($\mathbf{i}$ is a unit vector in the zonal direction). Equatorward of 3°, M is homogenized, so is ρ (at least below the thermocline), and thus $\|\nabla M\| \sim 0$, $\|\nabla\rho\| \sim 0$, and $\mathcal{Q}_E \sim 0$. This is consistent with observations of nearly-zero $\mathcal{Q}_E$ in the atmospheric troposphere (Hoskins, 1991) and in the mean equatorial subthermocline (Gouriou and Toole, 1993, Rowe *et al.,* 2000). At the poleward edges of this homogenized region, the strong barrier effect of the SSCCs, well documented by the above papers, is corroborated by strong gradients in $\mathcal{Q}_E$ (Fig. 6(c)). The homogeneous pool for the final $\mathcal{Q}_E$ (solid line in Fig. 6(c)) is much wider than the large-scale one (dashed line), as a consequence of the expulsion of gradients within the meridional cells. The homogenization and $\mathcal{Q}_E$ fronts are due to the combination of the planetary and relative potential vorticities (Fig. 6(d)). On the equatorward side of the jets, the relative potential vorticity $((g/\rho_0)J(u, \rho))$ compensates the planetary one $(-(g/\rho_0)\beta y\rho_z)$, yielding a flattening of $\mathcal{Q}_E$, where, within their cores, the two components add up to enhance the jump. In particular, without the shear term, the $\mathcal{Q}_E$ jump would be less pronounced, in agreement with Figure 8 of Rowe *et al.* (2000). Note however that the reversals of $\mathcal{Q}_E$ gradients near $|y| = 4°$ should trigger strong shear instability at the poleward edges of the jets. This is not taken into account in our strictly 2D model, but would take place in a fully 3D representation of the jet dynamics. The resulting eddy fluxes of heat and momentum would quickly modify the jet profile into a more stable form, and a weaker amplitude for the jet maxima would be obtained. Nevertheless the well-homogenized region should be void of instability even in a 3D representation.
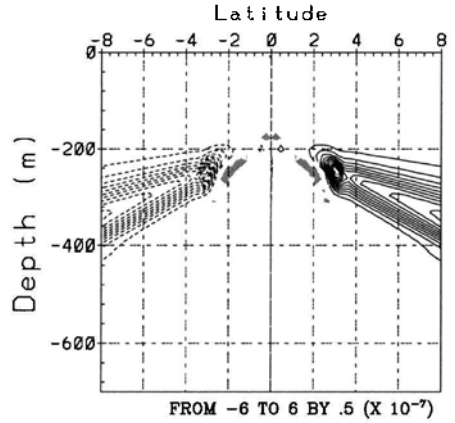
---

6. An average inertial instability time scale within the overturning cells is about 4–5 days (Coriolis parameter at $y = 1.5°$). Our choice of $\tau_\rho \geq 12$ days thus enables inertial instability to take place within the thermostad.
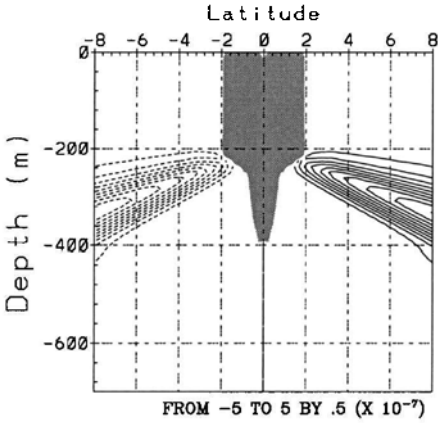
LARGE−SCALE PV   FINAL PV

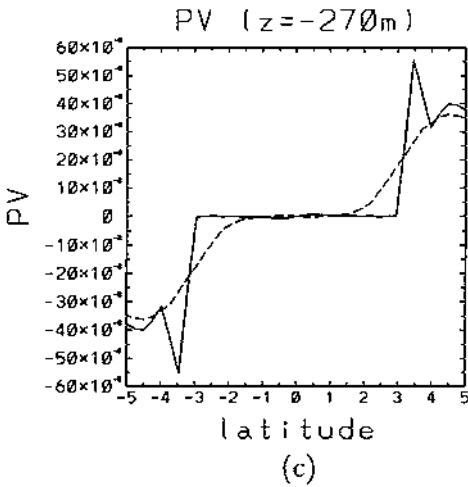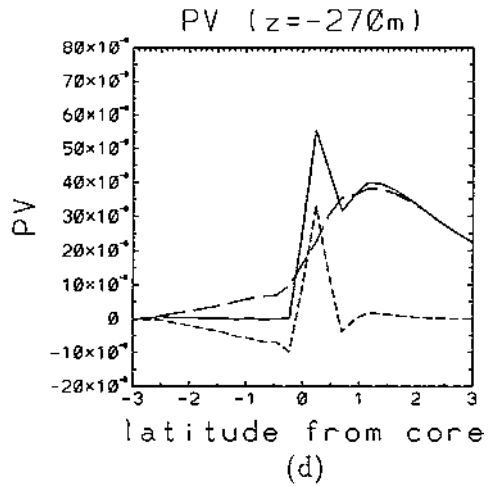(a)   (b)

(c)   (d)

Figure 6. Ertel potential vorticity Q_E for the same simulation as Figure 4: large-scale (a) and final (b) distributions (the zero isoline is long-dashed, and regions in grey correspond to $f Q_E < 0$); (c) latitudinal section at $z = -270$ m, with respect to geographic latitude, of the large-scale (dashed) and final (solid) Q_E; (d) latitudinal section at $z = -270$ m, with respect to the latitude from the core of the northern SSCC, of the final Q_E (solid) and of its relative (dashed) and planetary (long-dashed) components.

b. Case of westward surface flow

So far we have set $u_{SURF} = 0$, while observed surface currents are known to be westward in the vicinity of the equator. We shall study in this subsection the case where u_{SURF} is prescribed to be representative of the South Equatorial Current velocity,

$$u_{SURf}(y) = u_0 \left[1 - \tanh \left(\frac{|y| - y_s}{y_{EXT}} \right) \right] \bigg/ 2. \tag{28}$$

This profile is confined equatorward of $|y_s| = 600$ km and its poleward edges have a characteristic width $y_{EXT} = 600$ km. $u_0 = -25$ cm s^{-1}, so that the magnitude of the equatorial surface current is about -20 cm s^{-1} in the mixed layer.

Figure 7 presents the results obtained in that case. The most salient features are the weakening of the SSCCs amplitudes (65 cm s^{-1} versus 87 cm s^{-1} previously, Fig. 7(a)) and the modification of the lower part of the thermostad (Fig. 7(b)) to accommodate the strong deep westward flow at the equator. However SSCCs are still located at the same latitude, they are still mostly geostrophic (Fig. 7(d)) and the overturning cells are hardly modified (Fig. 7(c)). The corresponding meridional distributions of zonal velocity, isopycnal depth and Ertel PV support the same conclusions as in the previous subsection and are not shown here.

The weakening of the jets amplitude remains totally compatible with angular momentum preserving dynamics (Fig. 7(c)) and is such that

$$u_{SSCC} - \frac{\beta}{2} Y^2 \simeq u_{SURF}. \tag{29}$$

The SSCCs amplitude thus proves to be strongly modified by the value of the westward flow in the mixed layer.

We have tested the scaling law $Y^3 \propto \Delta\rho$ predicted in Section 2 (Eq. 12) for the latitude Y of the jets, by varying $\Delta\rho$ in a series of numerical simulations. The result is shown in Figure 8: the numerical estimates of Y (stars) follow the analytical prediction, within errors due to horizontal grid resolution of 20 km, when taking an effective density jump $(\Delta\rho)_{eff}$ across the thermocline region where $r_\rho > 0$ (dot-dashed line). The solid line corresponds to the case where $\Delta\rho$ is the total density jump across the thermocline.
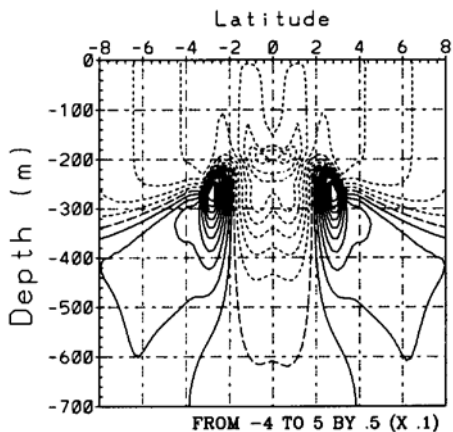
5. Interactions with the EUC

a. Rayleigh relaxation in density

In this section, the dynamics associated with the existence of a large-scale zonal pressure gradient, neglected in the previous section, is parameterized by a Rayleigh relaxation toward the following EUC profile
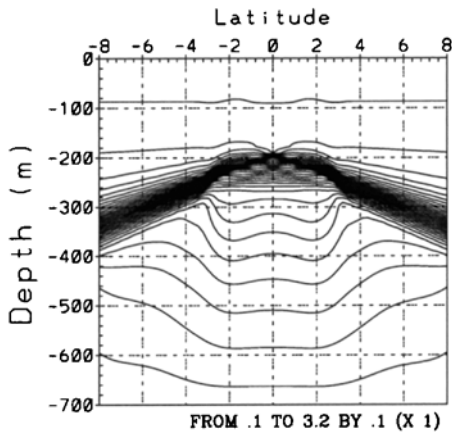
$$u_{EUC} = U_{EUC} \exp \left(-\frac{y^2}{2y_1^2} \right) \exp \left(-\frac{(z - z_0)^2}{2z_1^2} \right), \tag{30}$$
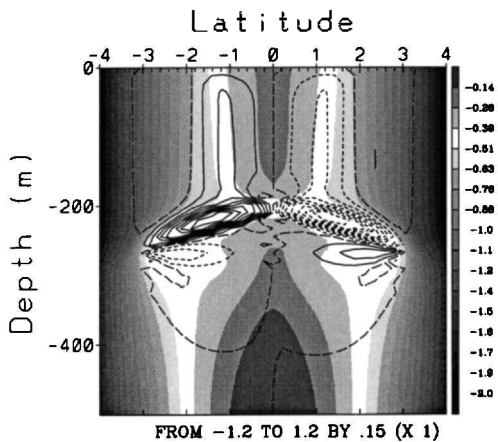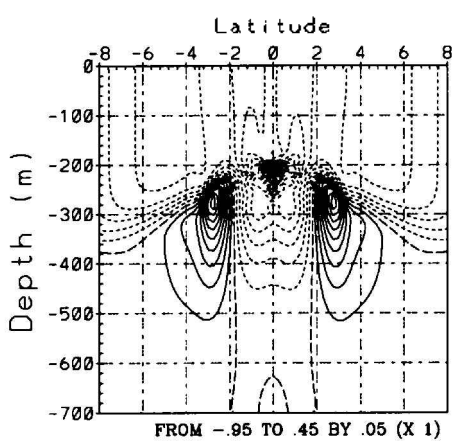
ZONAL VELOCITY

Latitude

Depth (m)

FROM −4 TO 5 BY .5 (X .1)

(a)

DENSITY

Latitude

Depth (m)

FROM .1 TO 3.2 BY .1 (X 1)

(b)

PSI + M

Latitude

Depth (m)

−0.14
−0.26
−0.39
−0.51
−0.63
−0.76
−0.88
−1.0
−1.1
−1.3
−1.4
−1.5
−1.6
−1.8
−2.0

FROM −1.2 TO 1.2 BY .15 (X 1)

(c)

GEOSTROPHIC VELOCITY

Latitude

Depth (m)

FROM −.95 TO .45 BY .05 (X 1)

(d)

Figure 7. Same as Figure 4 with u_{SURF} defined by (28) and without EUC.
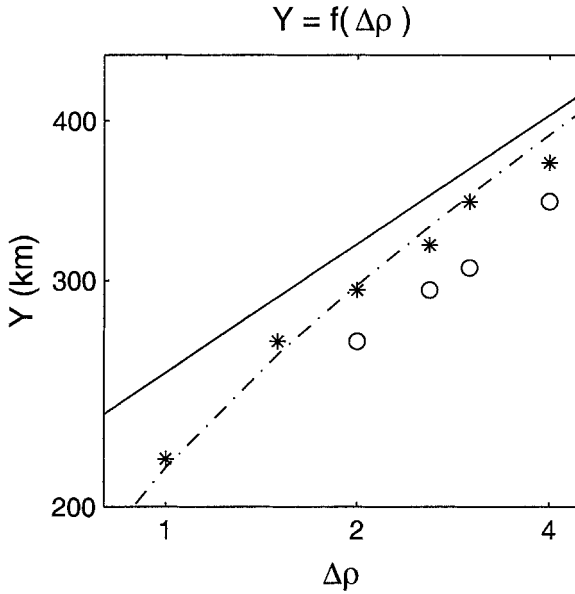
Figure 8. Log-log plot of jet position Y versus $\Delta\rho$: $Y = [(5g\alpha\Delta\rho)/(\rho_0\beta^2)]^{1/3}$ (solid), $Y = [(5g\alpha\Delta\rho_{EFF})/(\rho_0\beta^2)]^{1/3}$ (long-dashed) for an effective density jump $\Delta\rho_{EFF}$ across the thermocline region where $r_\rho > 0$, and results of numerical simulations without EUC (stars) and in the presence of an EUC (circles). In both simulations u_{SURF} is given by (28). No circles for $\Delta\rho < 2$ implies no eastward jet (for this choice of u_{SURF}).

with a maximum velocity equal to $U_{EUC} = 1$ m s^{-1} and a Gaussian profile centered at $z_0 = 230$ m, with latitudinal and vertical scales respectively of $y_1 = 70$ km and $z_1 = 30$ m. The value 1 m s^{-1} is a standard value for the EUC velocity in the Pacific, although it is an overestimate for the western region (Fig. 2(b) would yield $U_{EUC} = 0.40$ cm s^{-1}). The Rayleigh coefficient r_u is chosen with the same profile and a maximum amplitude R_u of 3×10^{-7} s^{-1}, which ensures that the relaxation term vanishes outside of the EUC region.

It is well known (e.g. Fig. 2) that the presence of an EUC has a geostrophic signature in density, corresponding to a splitting of the isopycnals within the thermocline at the equator. The previous run corresponds to an idealized case where ventilation theory applies up to $y = 0$, in the limiting case where the shadow zone intersects the equator in the westernmost part of the basin, implying no EUC and a poleward mass transport occurring entirely in the western boundary layer. The present section corresponds to the case where the shadow zone intersects the equator in the mid-basin, and mass balance requires the existence of an inertial EUC (Pedlosky, 1987), which is in thermal wind balance with the meridional density gradient. Accordingly the large-scale density field $\bar{\rho}$, shown in Figure 9(a), is now geostrophically consistent with the prescribed EUC (Eq. 30), and the Rayleigh relaxation term is adjusted to follow a given isopycnal of the large-scale density field (Fig. 9(b)).
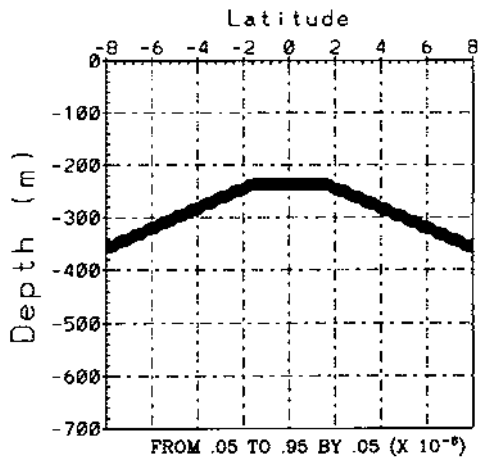
Since Subsection (4.b) yields more realistic SSCCs than (4.a), we continue to specify u_{SURF} with (28).

LARGE-SCALE DENSITY

(a)
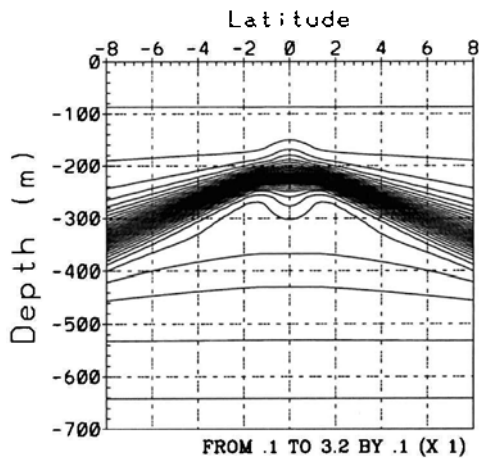
RAYLEIGH

(b)

Figure 9. Same as Figure 3, but in the presence of an EUC.

Figure 10 presents the numerical results in the presence of an EUC. The SSCCs still exist though with a weaker amplitude (47 cm s^{-1} vs 65 cm s^{-1} in Fig. 10(a)). They are slightly shifted toward the equator (2.7° vs 3.1°), but remain entities clearly separate from the EUC. Westward flow beneath the thermocline is very strongly reduced compared to Figure 7(a), which explains the flattening of the lower part of the thermostad near the equator (compare Fig. 7(b) and Fig. 10(b)). The thermocline overturning cells still exist as well, but they have a weaker amplitude and no longer reach the equator (Fig. 10(c)). Note that R_u stronger than 3×10^{-7} s^{-1} generates additional upwelling cells above the EUC, with a meridional extent similar to the EUC's (not shown). Again the lower part of the thermostad and of the jets results from geostrophic adjustment (Fig. 10(b,d)).

Figure 10(c) reveals that the upper branch of the thermocline overturning cells still tend to conserve angular momentum, but less efficiently when compared to Figure 7(c). The lower portion of the cells, by contrast, strongly interacts with the EUC, losing their conservative character. For $|y| < 2°$, the zonal velocity profile at $z = -270$ m is no longer quadratic in y (Fig. 11(a)), because of the EUC, while it remains quadratic for $2 < |y| < 3°$. Note however that the relative extent of these two regions would be affected by our choice for r_u.

The presence of the EUC flattens the large-scale density field $\bar{\rho}$, so that the available heat content which is redistributed is much less than in the previous cases (compare Fig. 11(b) to Fig. 5(b)). The overturning cells and thus the heat redistribution that they cause now occur only between 1° and 3° on either side of the equator, and the changes of slope between initial and final states are less pronounced. Finally $\mathcal{Q}_E$ is shown in Figure 12. General comments made in previous subsections still apply, even though the $\mathcal{Q}_E$ homogenization proves to be less efficient, with weaker meridional barriers in the range 250–300 m (compare Fig. 6(b) and Fig. 12(b)). In addition, the presence of the EUC translates into a horizontal barrier at the base of the thermocline (Fig. 12(a)–(b)), as in Gouriou and Toole (1993). That barrier still has a signature at 270 m between 1S and 1N (Fig. 12(c)). Besides, the large-scale $\mathcal{Q}_E$ field, computed with a geostrophic velocity that is set to zero at the bottom, is not as inertially unstable as in the case without EUC, suggesting that inertial instability plays a lesser role here. Note that Emanuel (1995) has shown that inertial instability strongly depends on the reference level for the geostrophic velocity, so that we cannot conclude whether inertial instability still triggers off the secondary circulation in the presence of a relaxation term toward the EUC in the x-momentum equation.

The dependence of the meridional extent Y for Hadley cells has been tested in the presence of an EUC (circles in Fig. 8), and the $(\Delta\rho)^{1/3}$-dependence still seems to hold, even though a shift in ordinate is observed. We can rationalize this shift by reapplying the analytical theory of Section 2 to a case where the shoaling of $\bar{\rho}$ flattens in the region of the EUC. Calling y_{EUC} the EUC's half-width, we obtain, in contrast with Eq. 12:

$$Y^3 = \frac{5g\alpha\Delta\rho}{\rho_0\beta^2}\left(1 - \left(\frac{y_{\text{EUC}}}{Y}\right)^2\right), \tag{31}$$

ZONAL VELOCITY

FROM −.25 TO .95 BY .05 (X 1)

(a)

DENSITY

FROM .1 TO 3.2 BY .1 (X 1)

(b)

Ψ′ and M

FROM −2.2 TO 2.2 BY .2 (X .1)

(c)

GEOSTROPHIC VELOCITY
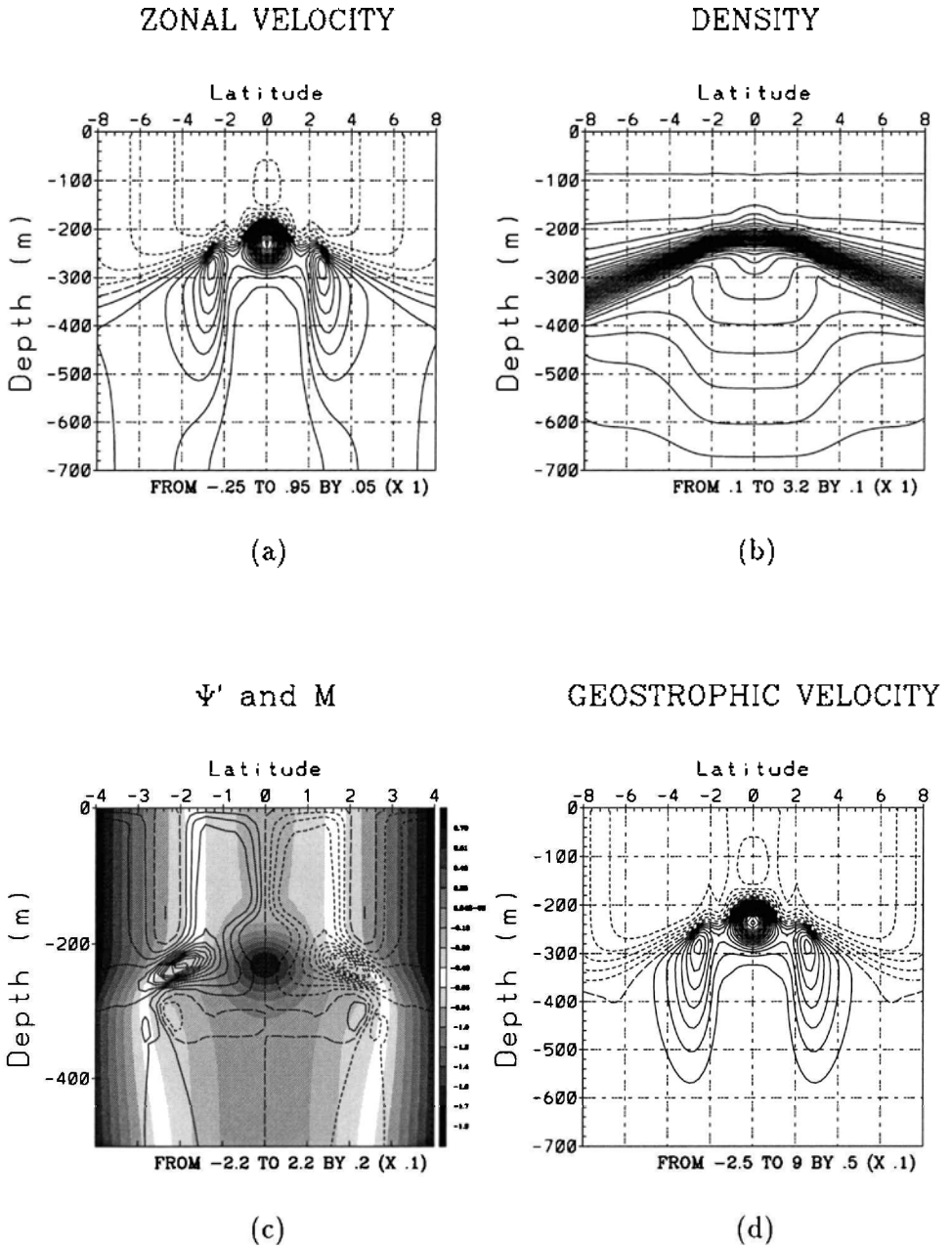

FROM −2.5 TO 9 BY .5 (X .1)

(d)

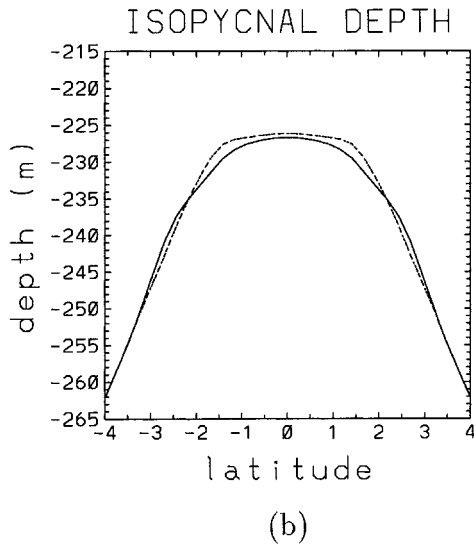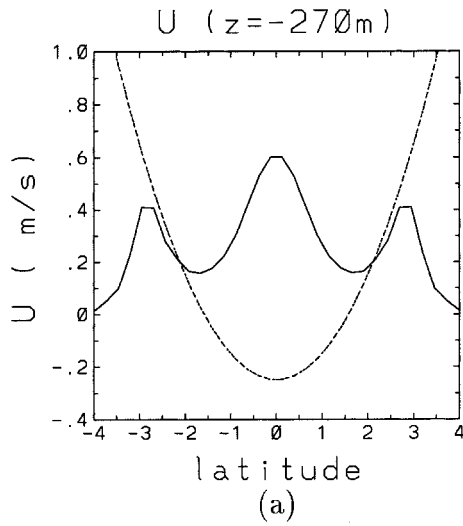Figure 10. Same as Figure 4, with u_{SURF} defined by (28) and in the presence of an EUC.
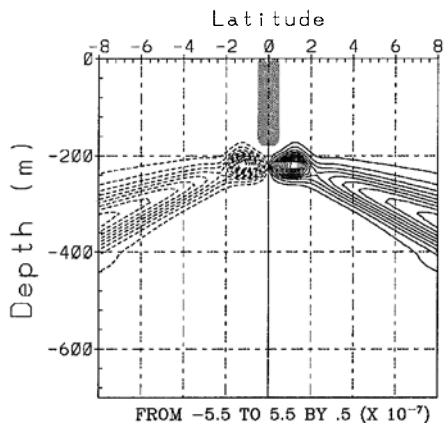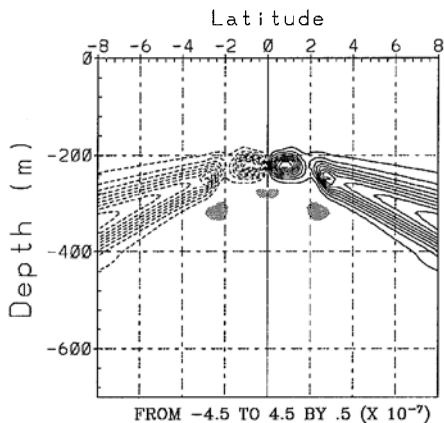
Figure 11. Same as Figure 5, with u_{SURF} defined by (28) and in the presence of an EUC.

LARGE−SCALE PV   FINAL PV

FROM −5.5 TO 5.5 BY .5 (X 10⁻⁷)   FROM −4.5 TO 4.5 BY .5 (X 10⁻⁷)

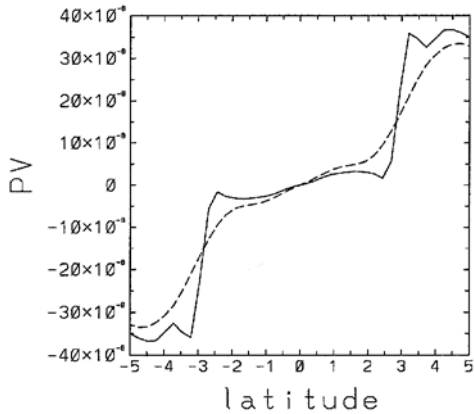(a)   (b)
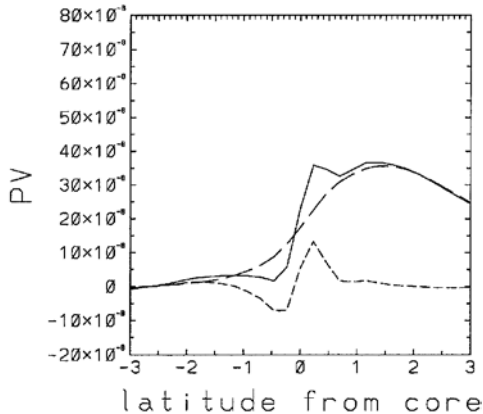
PV (z=−270m)   PV (z=−270m)

(c)   (d)

Figure 12. Same as Figure 6, for u_{SURF} defined by (28) and in the presence of an EUC.

which explains the $(\Delta\rho)^{1/3}$-dependence of Y and the vertical shift in Figure 8 for Y large enough compared to y_{EUC}.

b. *Dependence on the density forcing*

So far the density forcing is a Rayleigh relaxation, which has no spatial scale selection, and is restricted to the thermocline in order to parametrize the ventilated large-scale circulation.

In order to assess the influence of the vertical structure of the relaxation coefficient, Figure 13(a) and 13(b) present the solution found, in the presence of an EUC, for the extreme case of r_ρ constant throughout the whole domain. In this case, the SSCCs become z-independent below the thermocline, geostrophic adjustment cannot take place (since density is forced everywhere), and thus the deep isopycnals remain flat. Limiting the vertical extent of the relaxation region, therefore, proves crucial to simulating SSCCs with a finite vertical extent as well as a realistic deep thermostad.

Another way to force preferentially within the thermocline is to adopt, instead of $-r_\rho(z)(\rho - \tilde{\rho})$, a Laplacian scale-selective forcing $\kappa_z(\partial^2/\partial z^2)(\rho - \tilde{\rho})$. The resulting fields are shown for $\kappa_z = 10^{-3}$ m^2 s^{-1} in Figure 13(c)–(d) and present the same structure as in the Rayleigh relaxation case presented in Subsection 5a, namely the existence of SSCCs at the same latitude, although with a lesser amplitude, and the existence of a similar thermostad (see Fig. 10(a)–(b)).

From these two sets of solutions, we infer that the mechanism for the formation of SSCCs is largely independent of the details of the prescribed density forcing. The essential driving is actually the large-scale sloping of the thermocline; this has been confirmed by numerical solutions, not shown, where a flat large-scale thermocline produces no eastward jets distinct from the EUC. By contrast, the vertical structure of the SSCCs and the deep thermostad are sensitive to the choice of density forcing: forcing must become weak at subthermocline levels to obtain realistic results.

6. Discussion

With the same minimal assumptions as HH, we have rationalized the existence of the SSCCs and the meridional homogenization of temperature in the equatorial subthermocline observed in both the Atlantic and Pacific oceans. The forcing is the shoaling of the thermocline from the subtropics toward the equator due to large-scale ventilation, the analog of the meridional gradient of radiative balance temperature in the atmosphere. The mechanism is the redistribution and homogenization of angular momentum by secondary ageostrophic meridional cells located in the lower thermocline, the analogs of the Hadley cells. These cells also accomplish temperature homogenization, contributing to the overall structure of the equatorial thermostad. The SSCCs, at the poleward edges of that thermostad, appear as the oceanic counterparts of the Jet Streams.

Homogenization of angular momentum and of density results in nearly zero Ertel
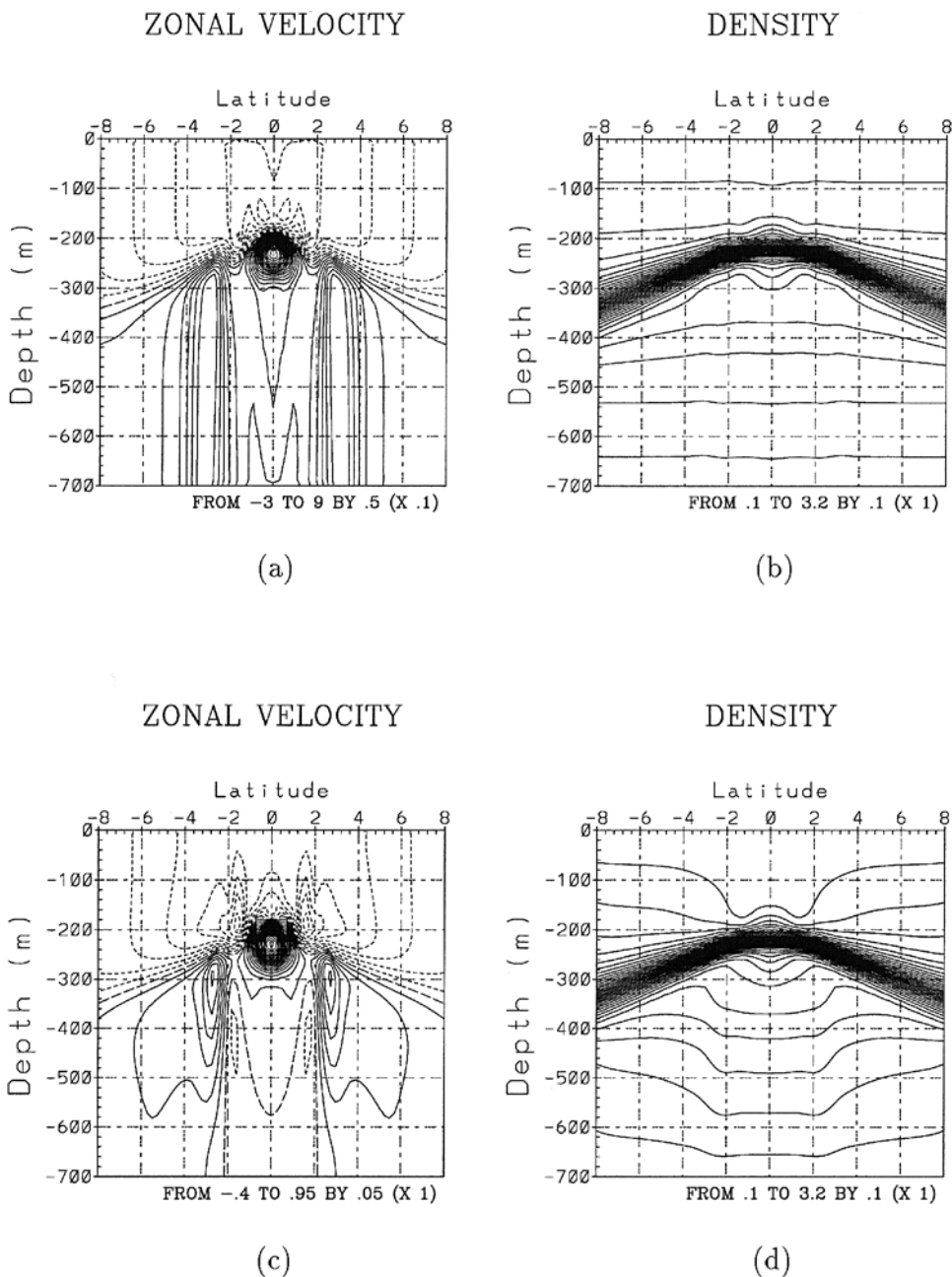
ZONAL VELOCITY

DENSITY

Latitude

Latitude

FROM −3 TO 9 BY .5 (X .1)

FROM .1 TO 3.2 BY .1 (X 1)

(a)

(b)

ZONAL VELOCITY

DENSITY

Latitude

Latitude

FROM −.4 TO .95 BY .05 (X 1)

FROM .1 TO 3.2 BY .1 (X 1)

(c)

(d)

Figure 13. Zonal velocity (a) and density field (b) for a constant r_ρ throughout the whole domain. Zonal velocity (c) and density field (d) for a Laplacian density forcing. Unit for velocity is m s^{-1} and density is given by $\rho - \rho_0 + \Delta\rho$.

potential vorticity in the lower thermocline and within the thermostad. Inertial instability may play a role in the rapid trigering of the equatorial secondary circulation. The homogenization of properties subsequently takes place within the closed streamlines of the meridional circulation, on a much longer time scale. Meridional gradients at the poleward edges of the lower (unforced) part of the thermostad are enhanced by geostrophic adjustment of the density field, a distinct feature of the oceanic case when contrasted to the atmospheric one, where no free geostrophic modes can be excited, the radiative forcing extending to the whole domain. As noted by Rowe *et al.* (2000), observations suggest the existence of strong diapycnal processes. Our ageostrophic cells provide a plausible mechanism for such diapycnal mixing.

We have seen that angular momentum is conserved, although more weakly, along the upper branch of the ageostrophic overturning cells even in the presence of an EUC, which implies that the amplitude of the SSCCs depends on the strength of the westward flow in the surface layer. This nearly inviscid nonlinear mechanism is fundamentally different from McPhaden's (1984) diffusive theory. In the presence of an EUC, the overall structure of the solutions remains the same, although homogenization is weaker, yielding eastward jets still distinct from the EUC, but of lesser amplitude, and meridional cells of lesser width.

An important implication of this paper is that the geostrophic balance for the zonal momentum, one building block of the ventilation theory, fails at a distance of about 3° latitude from the equator, i.e. a distance wider than the inertial half-width of the EUC. This distance corresponds to the meridional extent of the thermocline overturning cells and closely depends on the equatorial radius of deformation. Equatorward of 3° latitude, one must superimpose to geostrophic dynamics an ageostrophic circulation that tends to conserve angular momentum, in analogy with the atmospheric case.

Another important implication of this paper is that the SSCCs are not the consequence of, but the cause for, importing water masses from high latitudes. The dynamics described above are local, in that the large-scale thermocline slope, thermocline thickness and equatorial radius of deformation at a given longitude determine the latitude and depth of the eastward jets at that longitude. The latitude and depth at which water must be extracted from the western boundary to satisfy zonal continuity is therefore determined by down-stream rather than upstream factors.

The first obvious limitation of our approach is the essentially 2D framework which has been chosen for the secondary circulation. Previous studies of the axi-symmetric atmospheric circulation have shown that such a formulation yields about the right geometry for the Hadley cells, but Jet Streams with too large an amplitude. As remarked in Section 4a, the jet profiles found in our 2D simulations are obviously prone to shear instability on their poleward flanks and would reach a weaker amplitude in a fully 3D model. Since the dependence on longitude of our 2D formulation is purely parametric, another issue we cannot address is the zonal evolution of the SSCCs (y, z)-structure caused by the eastward shoaling of the thermocline, as studied by Johnson and Moore (1997). In a 3D case, the

implied zonal stretching would contribute to the determination of the latitude and depth of the SSCCs, as do the local parameters mentioned above.

Another limitation of our approach is that we are looking for steady state solutions which are supposed to be representative of the time-mean equatorial circulation, while the observed flows are not steady (see Rowe *et al.* (2000)). Finally, our model is completely symmetric about the equator, while the seasonal asymmetry of the Hadley cells about the equator plays a quantitative role in the atmospheric case. The effects of meridional asymmetry and of zonal dependence are under study and will be addressed subsequently.

REFERENCES

Batchelor, G. K. 1956. Steady laminar flow with closed streamlines at large Reynolds number. J. Fluid Mech., *1,* 177–190.

Cessi, P. 1998. Angular momentum and temperature homogenization in the symmetric circulation of the atmosphere. J. Atmos. Sci., *55,* 1997–2015.

Condie, S. A. and P. B. Rhines. 1994. Topographic Hadley cells. J. Fluid Mech., *280,* 349–366.

Defant, A. 1936. The troposphere-scientific results of the German Atlantic expedition of the research Vessel ''*Meteor*'' 1925–27, vol. VI, part 1. English translation 1981, W.J. Emery, ed., Amerind Publishing Co, New Delhi.

Delcroix, T., G. Eldin, M. H. Radenac, J. M. Toole and E. Firing. 1992. Variation of the western equatorial Pacific Ocean. J. Geophys. Res., *97,* 5423–5445.

Emanuel, K. A. 1995. On thermally direct circulations in moist atmospheres. J. Atmos. Sci., *52,* 1529–1534.

Gouriou, Y. and J. Toole. 1993. Mean circulation of the upper layers of the western equatorial Pacific Ocean. J. Geophys. Res., *98,* 22495–22520.

Held, I. M. and A. Y. Hou. 1980. Nonlinear axially symmetric circulations in a nearly inviscid atmosphere. J. Atmos. Sci., *37,* 515–533.

Hide, R. 1969. Dynamics of the atmospheres of the major planets with an appendix on the viscous boundary layer at the rigid boundary surface of an electrically conducting rotating fluid in the presence of a magnetic field. J. Atmos. Sci., *26,* 841–853.

Hoskins, B. J. 1991. Towards a PV-θ view of the general circulation. Tellus, *43 AB,* 27–35.

Hua, B. L., D. W. Moore and S. Le Gentil. 1997. Inertial nonlinear equilibration of equatorial flows. J. Fluid Mech., *331,* 345–371.

James, I. N. 1994. Introduction to Circulating Atmospheres, Cambridge University Press, 422 pp.

Johnson, G. C. and D. W. Moore. 1997. The Pacific subsurface counter-currents and an inertial model. J. Phys. Oceanogr., *27,* 2448–2459.

Lindzen, R. S. 1990. Dynamics in Atmosphere Physics, Cambridge University Press, 310 pp.

Lindzen, R. S. and A. Y. Hou. 1988. Hadley circulations for zonally averaged heating centered off the equator. J. Atm. Sci., *45,* 2416–2427.

Liu, Z. 1994. A simple model of the mass exchange between the subtropical and tropical ocean. J. Phys. Oceanogr., *24,* 1153–1165.

Luyten, J. R., J. Pedlosky and H. Stommel. 1983. The ventilated thermocline. J. Phys. Oceanogr., *13,* 292–309.

McCreary, J. P. Jr. and P. Lu. 1994. Interaction between the subtropical and equatorial ocean circulations: The subtropical cell. J. Phys. Oceanogr., *24,* 466–497.

McPhaden, M. J. 1984. On the dynamics of equatorial subsurface countercurrents. J. Phys. Oceanogr., *14,* 1216–1225.

Pedlosky, J. 1987. An inertial theory of the equatorial undercurrent. J. Phys. Oceanogr., *17,* 1978–1985.

—— 1988. Entrainment and the termination of the equatorial undercurrent. J. Phys. Oceanogr., *18,* 880–886.

—— 1996. Ocean Circulation Theory, Springer, 460 pp.

Philander, S. G. H. and R. C. Pacanowski. 1980. The generation of equatorial currents. J. Geophys. Res., *85,* 1123–1136.

Rowe, D. G., E. Firing and G. C. Johnson. 2000. Pacific equatorial subsurface countercurrents' velocity, transport, and potential vorticity. J. Phys. Oceanogr. (in press).

Tsuchiya, M. 1972. A subsurface north equatorial countercurrent in the eastern Pacific Ocean. J. Geophys. Res., *77,* 5981–5986.

—— 1975. Subsurface countercurrents in the eastern equatorial Pacific Ocean. J. Mar. Res., *33,* 145–175.

—— 1981. The origin of the Pacific Equatorial 13°C Water. J. Phys. Oceanogr., *11,* 794–812.

—— 1986. Thermostads and Circulation in the Upper Layer of the Atlantic Ocean. Prog. Oceanogr., *16,* 235–267.

Tsuchiya, M., L. D. Talley and M. S. McCartney. 1994. Water-mass distributions in the western South Atlantic; A section from South Georgia Island (54S) northward across the equator. J. Mar. Res., *52,* 55–81.

Wyrtki, K. and B. Kilonsky. 1984. Mean water and current structure during the Hawaii-to-Tahiti Shuttle experiment. J. Phys. Oceanogr., *14,* 242–254.